Erasmus Mundus Joint master's degree

in Surface, Electro, Radiation, and Photochemistry

Master thesis

Preparation and characterization of microporous layers by phase inversion technique and Cyrene as a green solvent

Quyen Do

Supervisor:

Professor Antonio Comite

Hosting Institution

Department of Chemistry and Industrial Chemistry, School of

Mathematical, Physical and Natural Sciences, University of Genoa

July 2022

This page intentionally left blank.

Table of Contents

Abstract: Preparation and characterization of microporous layers by phase inversion technique and Cyrene as a green solvent

Organic solvents, such as N, N-dimethyl formamide (DMF), or N-Methyl pyrrolidone (NMP) have been used for the microporous layer (MPL) preparation applying to Polymer electrolyte membrane fuel cells (PEMFC). Unfortunately, these are all toxic organic solvents which result in human health and environmental risks. In this work, Cyrene^{TM} was employed as a green solvent to dissolve poly(vinylidenefluoride) (PVDF), the solution was then mixed with Carbon black (CB) as filler. The MPL was fabricated by nonsolvent-induced phase separation technique (NIPS). The experimental data were discussed with respect to the ternary phase diagram, contact angle, roughness, morphology, porosity, and pore size distribution. Influence of polymer/filler ratio and coagulation bath conditions on characteristics of the MPL was thoroughly analyzed.

Key words: *Green solvents, PEMFC, Microporous layer, NIPS*

Sommario: Preparazione e caratterizzazione di strati microporosi mediante la tecnica di inversione di fase e Cyrene come solvente "green". Le celle a combustibile con membrana a scambio protonico (PEMFC)

Solventi organici, come N, N-dimetilformammide (DMF) o N-metil pirrolidone (NMP) sono stati utilizzati per la preparazione di strati microporosi (MPL) da applicare in celle a combustibile a membrana elettrolitica polimerica (PEMFC). Sfortunatamente, questi sono tutti solventi organici tossici che comportano rischi per la salute umana e per l'ambiente. In questo lavoro, Cyrene^{TM} è stato impiegato come solvente "verde" per sciogliere il poli(vinilidene fluoruro) (PVDF), la soluzione è stata quindi miscelata con nerofumo (CB) come riempitivo. Il MPL è stato sintetizzato mediante la tecnica di inversione di fase indotta da non solvente (NIPS). I dati sperimentali sono stati discussi rispetto al diagramma di fase ternario, all'angolo di contatto, alla rugosità, alla morfologia, alla porosità e alla distribuzione delle dimensioni dei pori. L'influenza del rapporto polimero/riempitivo e delle condizioni del bagno di coagulazione sulle caratteristiche dell'MPL è stata analizzata in dettaglio.

Parole chiave: *Solventi "green", PEMFC, Strato microporoso, NIPS*

Acknowledgment

Firstly, I would like to express my immense appreciation to my extraordinary supervisor, Professor. Antonio Comite, for giving me a great opportunity in the “membrane & membrane” group. You are a very kind professor; I say from what I saw and felt during the long time we worked together. I greatly appreciate your scientific support and your time during the six months I have been working here. I also thank Dr.Marcello Pagliero, for his kindness, guidance and consistent assistance. He taught me most of the techniques I used while working on the project which I will always be grateful for. I also want to thank Ms. Ilaria Rizzardi for her unconditional assistance during my stay at the lab. I thank my fellow labmates Ms. Reshma, Mr. Ermias, Ms. Georgia, Mr. Massimo, Mr. Matteo, Mr. Andrea, Ms. Fiorenza, Ms. Raffaella, for the stimulating discussions, for working together, and for all the fun we have had in the last six months.

I especially thank Professor Sandrine Lacombe (Université Paris-Saclay), Professor Edouardo Marques (University of Porto), and Professor Mario Rocca (University of Genoa) for your help, guidance, suggestion, and encouragement throughout the whole SERP+ program. I also like to thank Ms. Eva Renouf, Ms Mariachiara Lupi and Mr. Kalidiouma Sidibe for the unconditional administrative assistance during the program.

Besides my advisor, I would like to thank European Commission and SERP+ program for giving me this precious opportunity to have my higher education in an interdisciplinary study. Thank all of the students in the SERP+ 2020-2022 program for our wonderful time together. You all are the best students I have ever known. No matter what you will do after graduation, I hope we could get more successful in the future.

Also, I thank my friends in the following institution: Université Paris-Saclay, Universidade Do Porto, and Università degli Studi di Genova for a great time with you in three universities and three countries; my beloved friends Serrano Marti-nez Marta, Le Quy Hien, Pham Ba Lich, Nguyen Hai Dang, Pham Trong Thuy, Chopra Cheshta, Qian Jianan, Horbenko Yuliia, and Do Thuy Linh for all the good times we had together.

I would like to thank my family: my parents and my brothers for supporting me spiritually throughout writing this thesis and my life in general.

Finally, I dedicate this thesis book to Hung Quoc Nguyen who is doing PhD at NTNU, Norway for helping me with unconditional love since I was in my undergraduate. Both you and I all faced thousands of obstacles stuff but we always hand in hand to overcome and escape from our own comfort zone.

List of abbreviations

CB	Carbon black
CL	Catalyst layer
Cyrene^{TM}	Dihydrolevoglucosenone
DMA	N, N-dimethyl acetamide
DMF	Dimethylformamide
GDL	Gas diffusion layer
KDa	Kilodalton
MPL	Microporous layer
MEA	Membrane electrode assembly
NIPS	Non-solvent Induced Phase Separation
PEM	Polymer electrolyte membrane
PEMFC	Polymer electrolyte membrane fuel cells
PVDF	Polyvinylidene fluoride
PTFE	Polytetrafluoroethylene
PFSA	Perfluoro sulphonic acid

Chapter 1: Introduction

Environmental pollution and global warming issues are consequences of conventional power generation systems which are based on fossil fuels. This has motivated the research and development toward clean, new, and robust power generation devices. Among them, fuel cells have been considered as an alternative candidate for electrical energy sources nowadays. There are various kinds of fuel cells, however, proton exchange membrane fuel cells (PEMFC) have attracted the most attention due to their high power density and low operating temperature[1].

In PEMFC systems, gas diffusion layers (GDL) play an important role to transport the reactant gases and provide the needed electrical conductivity. A GDL normally consists of a microporous layer (MPL) and supporting substrate. The MPL distributes the reactants and ensures an effective electrical contact with the catalyst layer while facilitating the liquid water expulsion through its hydrophobic character. Usually, expensive polytetrafluoroethylene (PTFE) is used as hydrophobic agent and recently also other easier processable polymers have been proposed as polyvinylidene difluoride (PVDF). In order to fabricate the microporous layer, firstly polymer or mixture of polymers needs to be dissolved by a solvent. Currently, organic solvents, such as N, N-dimethyl acetamide (DMA), N, N-dimethyl formamide (DMF), and N-Methyl pyrrolidone (NMP) have been used for the MPL preparation since these above-mentioned solvents show excellent ability to dissolve polymeric materials. Unfortunately, these are all toxic organic solvents which result in human health and environmental risks[2]. Hence, green solvents need to be considered to replace the toxic solvents.

In this study, dihydrolevoglucosenone (Cyrene^{TM}) was used as green solvent to dissolve polyvinylidene fluoride (PVDF), the solution was then mixed with Carbon black (CB) as electroconductive filler. The MPL was fabricated by phase separation-based method. Influence of polymer/filler ratio and coagulation bath conditions on characteristics of the MPL was thoroughly analyzed.

1.1 Polymer electrolyte membrane fuel cell (PEMFC)

During recent decades, the proton exchange membrane fuel cells (PEMFCs) have been considered as the promising power sources due to their high-power density and low-temperature operation which show an excellent performance in both stationary and portable applications[3, 4]. Membrane-electrode assembly (MEA) plays an important role in the fuel cell system. This crucial part consists of electrodes, electrically conductive porous gas diffusion layers (GDL), catalyst layers, and ion-conducting electrolyte[3], as shown in Figure 1.

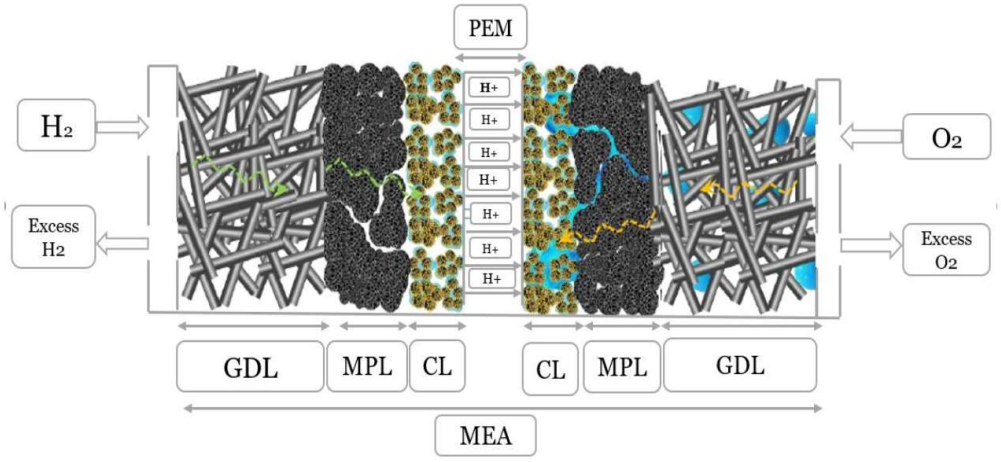

Figure 1: Schematic diagram of PEMFC structure[5]

In principle, fuel (hydrogen) is supplied to anode side, while air (oxygen) is supplied to cathode side. Hydrogen is oxidized to produce the negatively charged electrons and the positively charged protons. The electron is then transferred to an external circuit connected to cathode. In the meantime, the proton passes through hydrated PEM to the cathode where reaction takes place by the combination of the proton, the electron, and the oxygen. Herein, the oxygen is reduced by the electrons and then combined with the protons to produce heat and water. The water can be formed in either gaseous or liquid state depending on the operation temperature of the fuel cell system. The operating principles of a PEMFC can be illustrated in Figure 2.

Hydrogen oxidation (at anode): $H_2 \rightarrow 2H^+ + 2e^-$

Oxygen reduction (at cathode): $\frac{1}{2}O_2 + 2H^+ + 2e^- \rightarrow H_2O$

Overall reaction: $H_2(g) + \frac{1}{2}O_2(g) \rightarrow H_2O(g/l)$

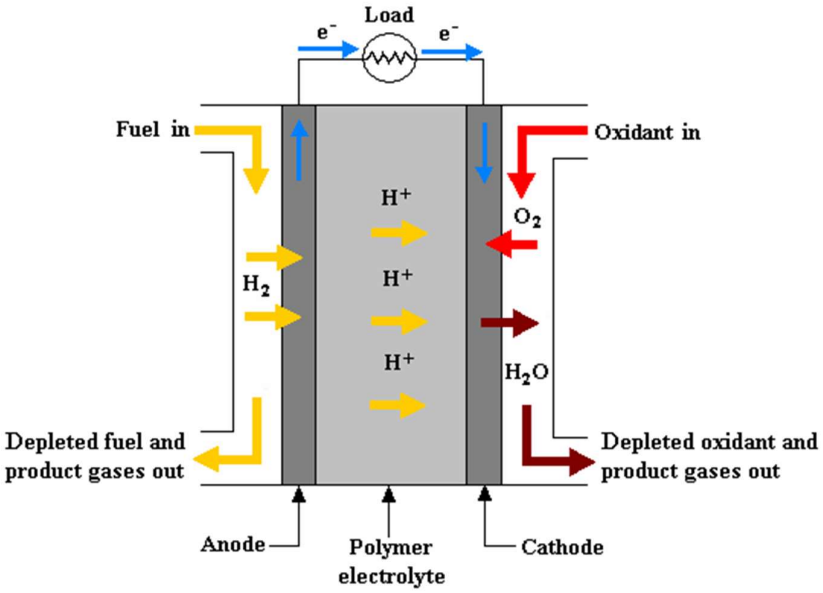

Figure 2: Schematic diagram of PEMFC operation[6]

1.2 Polymer electrolyte membrane (PEM)

The polymer electrolyte membrane, or proton-exchange membrane (PEM), is made from ionomers and its function is to conduct protons and block electrons pathway through the membrane. Among available PEM materials, perfluorosulphonic acid (PFSA)-based polymer (Nafion®) is the most common material which is produced by DuPont[7]. Nafion® is an ionomer containing a perfluorinated backbone attached with sulphonic acid group. Thanks to the fixed charge sites, the protons can be transported inside the membrane. It should be noted that the PEM must be saturated with water to be able to conduct protons.

1.3 Catalyst layer (CL)

The catalyst layer is where electrochemical reactions take place, this layer consists of metal Platinum (Pt) with particle size of 2-4 nm[8]. Catalyst particles require to have contact with both electronic and protonic conductors in order to catalyze reactions. Surface area of the catalyst plays an important role to efficiency of the catalyst layer. The smaller the Platinum particles, the larger the its active surface area is, which increase the system performance.

1.4 Gas diffusion layer (GDL)

The gas diffusion layer (GDL) is assembled between the flow field and the catalyst layer inside the PEMFC in order to transport the reactant gases and provide the electrical conductivity. To possesses these two main functions, an ideal GDL should consist of a macro-porous Carbonbased substrate (e.g. either carbon paper or cloth) and a microporous layer, as illustrated in Figure 3.

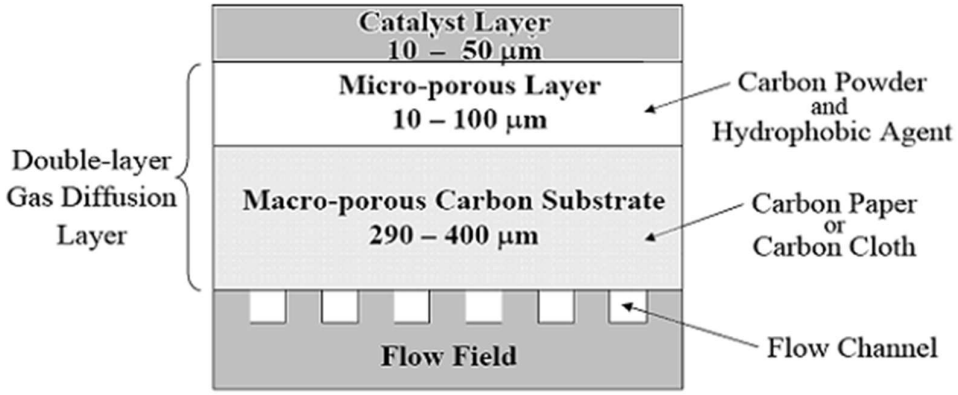

Figure 3: A cut away GDL schematic for the PEMFC system[9]

1.5 Microporous layer (MPL)

The microporous layer (MPL) is normally casted with a very thin thickness of about 10-100 μm onto either Carbon paper or Carbon cloth. The addition of the MPL is to prevent water flooding and increase pathways for the transportation of the reactant gases[10]. Furthermore, the MPL is added to reduce electrical resistance in the PEMFC system and also prevent damaging the catalyst layer induced by Carbon fibers contained in the Carbon substrate[11].

Composition of the MPL consists of a hydrophobic polymer as binder and Carbon-based nanoparticles as filler. Polytetrafluoroethylene (PTFE) and polyvinylidene fluoride (PVDF) are two common polymers used as hydrophobic binders. However, PTFE is insoluble in almost all solvents and it is applied as a dispersed solid phase or emulsion[12]. In issue of the use of PTFE heterogeneous formulation is related to its homogeneous and reliable distribution in the MPL, beside its higher costs. Thanks to easier dissolution in common organic solvents, PVDF is usually used as binder instead of PTFE. Containing the PVDF assists the MPL possessing hydrophobicity to avoid water flooding while adding Carbon-based nanoparticles provides the electrical conductivity for the MPL films. Optimizing the concentration of binder and the loading content of the filler in dope solution is needed to achieve a good performance for PEMFC application.

1.6 Non-solvent Induced Phase Separation Process (NIPS)

In this work an alternative method commonly used for the manufacture of porous polymeric membranes has been adopted for preparation of the MPL. Polymeric porous membranes are normally produced by phase separation-based fabrication methods. These techniques include temperature induced phase separation (TIPS), solvent evaporation induced phase separation (EIPS), non-solvent induced phase separation (NIPS), and vapor induced phase separation (VIPS). Among the above-mentioned methods, non-solvent induced phase separation (NIPS) is the most applied approach to fabricate polymeric membrane with porous structure and high selectivity at low operation temperature.

Firstly, a dope solution is prepared by dissolution of polymer in solvent and mixture with other additives. The dope solution is then cast on a flat substrate as a liquid film which is immersed into a

coagulation non-solvent bath. Herein, the solvent in the liquid film exchanges with the non-solvent in the coagulation bath, the phase separation process takes place inducing the MPL formation[13].

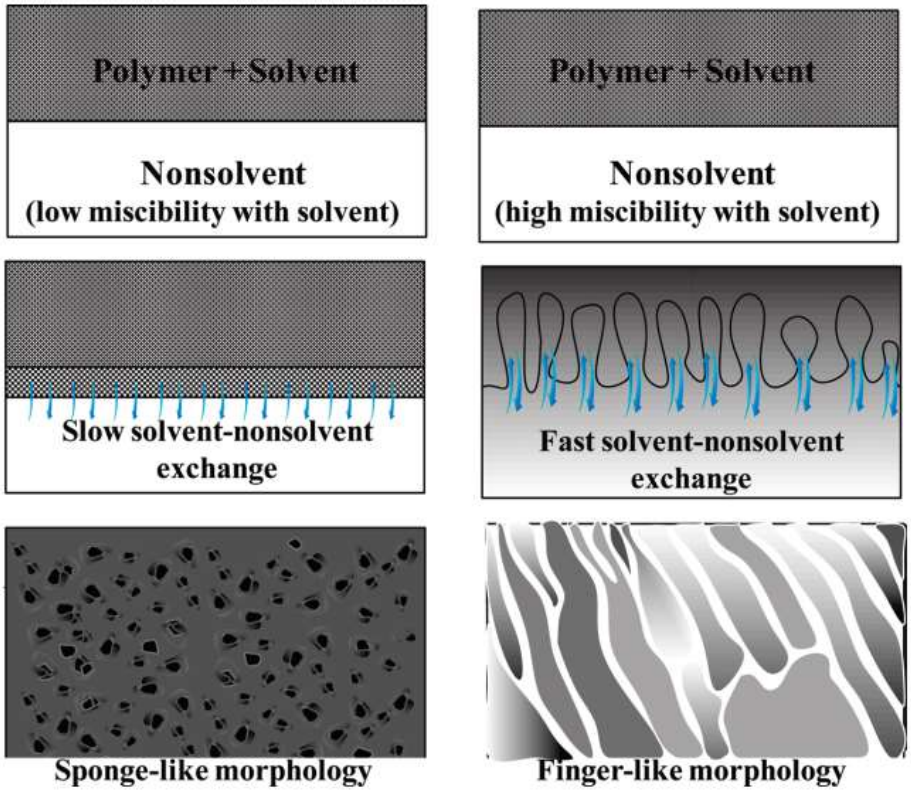

Figure 4: Different types of demixing inducing different membrane morphologies[14]

The choice of solvent-nonsolvent system has a dramatic influence on morphology and porosity of the membrane. The solvent and nonsolvent must be miscible in order to facilitate occurring the exchange process. How the miscibility of nonsolvent with solvent impacts on the membrane morphology can be illustrated as shown in Figure 4. The higher the miscibility of nonsolvent with solvent, the faster the solvent-nonsolvent exchange process occurs[14]. The fast exchange induces to form the membrane with finger-like morphology while the membrane with sponge-like substructure is obtained in the case of low exchange rate.

1.7 Cyrene™ as green solvent

Dihydrolevoglucosenone (Cyrene™) is a bio-based solvent, derived from cellulose via two simple steps, developed by Circa Group collaborating with Professor J.Clark[15]. Cyrene™ can be used as green solvent to substitute hazard solvents which are employed to dissolve fluoropolymers (PVDF).

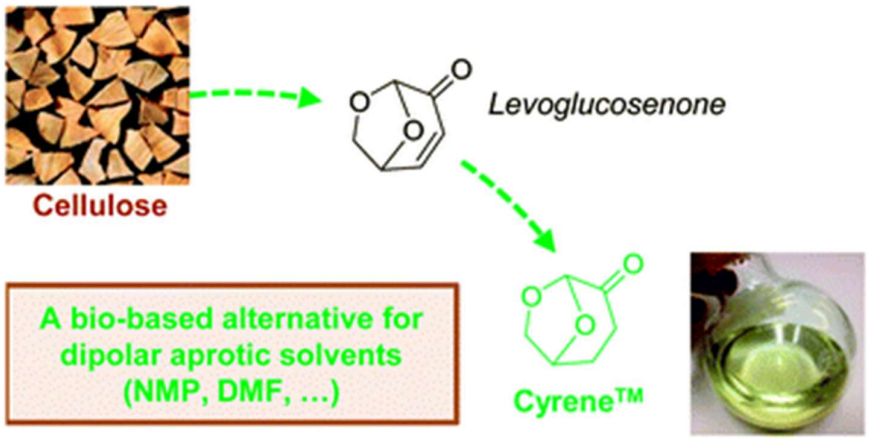

Figure 5: Dihydrolevoglucosenone (Cyrene™)[15]

Cyrene™ possesses a polarity similar to NMP without containing N-alkyl amide group in its structure[16]. Therefore, this type of solvent is safer to handle and environmental friendly since its degradation products are only water and carbon dioxide.

1.8 Polymer dissolution

Polymer dissolution can be governed by both kinetic and thermodynamic effects[17]. The dissolution process involves several diffusion stages of the liquid solvent into the solid polymer matric until the whole polymer chains are dissolved, as shown in Figure 6. The process can be accelerated by heating the mixture of polymer and solvent. Also, the duration of dissolution process could facilitate dissolving the given polymer.

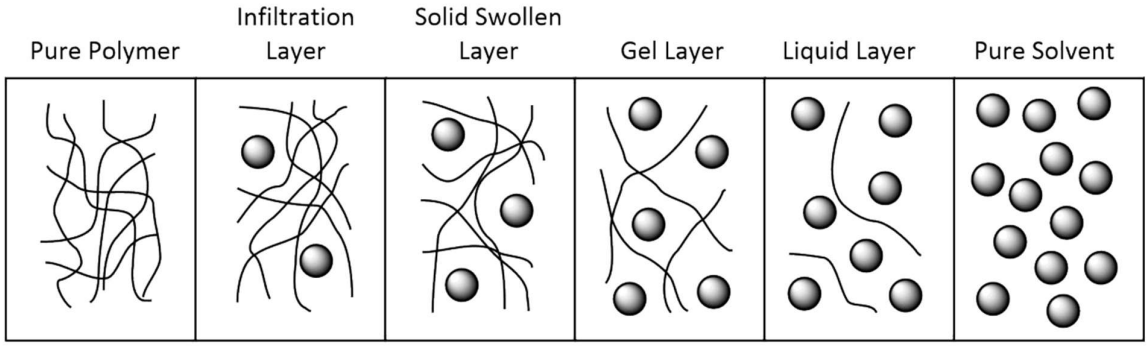

Figure 6: Stages of polymer dissolution, illustrating intermediate layers between a pure polymer and a pure solvent[17].

Chapter 2: Materials and Methods

2.1 Materials

Polyvinylidene fluoride (PVDF) polymer possessing a molecular weight of 430KDa (Foraflon 1000HD) was supplied to the research group by Atochem (now Arkema). Dihydrolevoglucosenone (Cyrene®) (>99%) was provided from Sigma Aldrich, Germany. Carbon black (CB) powder (Ketjenblack EC-300J) (Alfa Aesar, Italy) was used as electrically conductive filler. In order to fabricate the microporous layers, the non-solvents deionized water and ethanol (Carlo-Erba, Italy) were employed for coagulation bath. A 145µm carbon paper (AVCARB style 2002HD, USA) was used as a support substrate.

2.2 Microporous layer preparation

The PVDF polymer was firstly dispersed in Cyrene and the mixture was stirred for 1 hour at 80 °C in order to achieve complete dissolution. Carbon black used as electrically conductive filler was added to the polymeric solution, the dispersion was then stirred for at least 3 hours to obtaining a homogeneous slurry. In the next step, the polymer-filler solution was successively cast onto the commercial carbon paper. The film was immediately immersed into a coagulation bath with water as nonsolvent for 10 minutes in order to form the microporous layer by solvent-nonsolvent exchange. The cast film was rinsed with deionized water to remove any contaminants, then dried at room temperature overnight as final step.

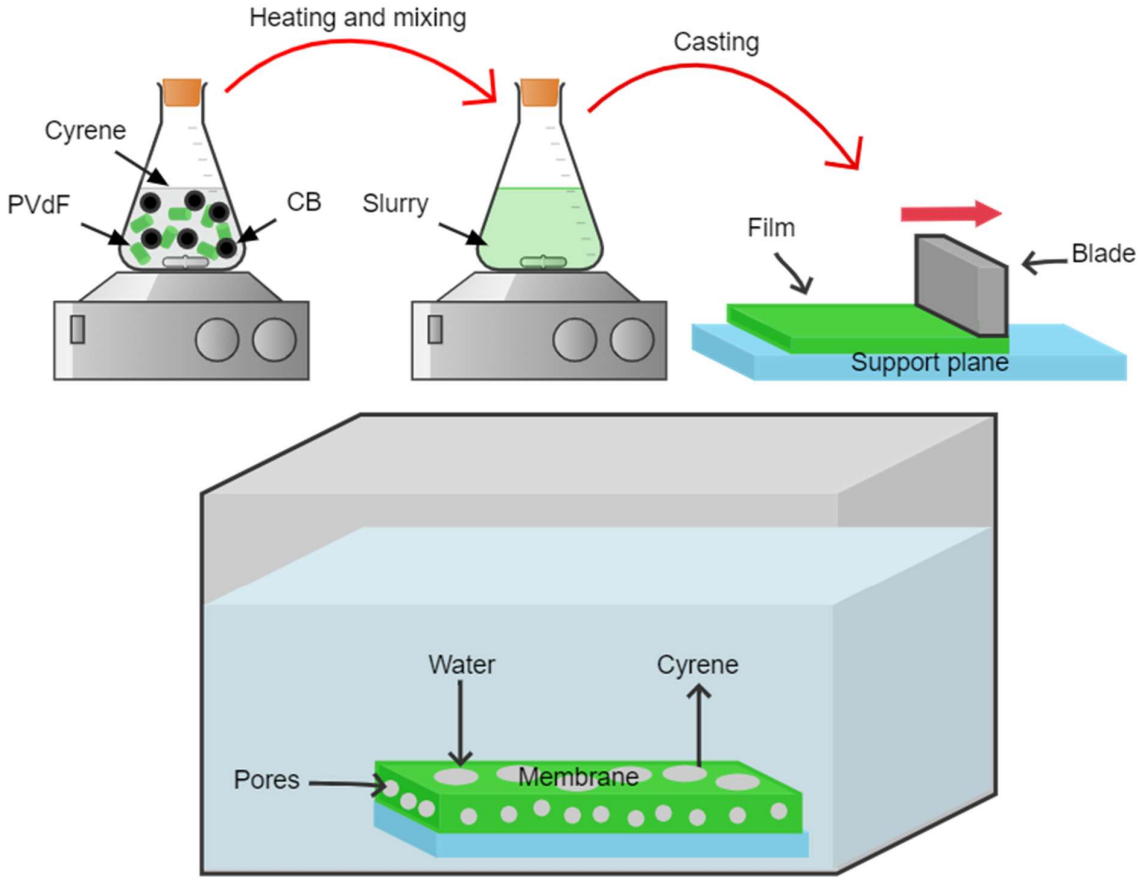

Figure 7: Schematic illustration of MPL membrane fabrication

2.2.1 Preparation of the MPL samples with different CB:PVDF ratios

The ratio of CB and PVDF is a key factor to optimize the hydrophobicity and electrical conductivity. In this experiment, the concentration of PVDF was maintained with 12 wt. % in the slurry while the content of CB was added as a variation. Five different ratios of CB:PVDF were performed as 1:5, 1:7, 1:9, 1:11, and 1:15. The MPL preparation was followed by the above-mentioned protocol.

2.2.2 Preparation of the MPL samples with different coagulation bath conditions

By using non-solvent induced phase separation, the coagulation bath condition was then considered as an important role in the solvent-nonsolvent exchange process. The MPL samples were prepared with the different conditions of coagulation bath which is shown as Table 1.

Table 1: The MPL samples with different coagulation bath conditions

Abbreviation	Coagulation bath conditions
W	Using Water as non-solvent
E	Using Ethanol 96% as non-solvent
W.E	Using mixture of Water and Ethanol (1:1) as non-solvent
W.HT	Using high-temperature Water (50 °C) as non-solvent
W.LT	Using low-temperature Water (2 °C) as non-solvent

2.3 Microporous layer Characterization

2.3.1 Cloud point measurements

In order to investigate polymer/solvent/nonsolvent (PVDF/Cyrene/Water) interactions, the ternary phase diagram was drawn with the cloud point curve. In this report, the cloud point curve was obtained through a titration method. First, the solutions of PVDF/Cyrene were prepared with five different concentrations of PVDF. These five different polymeric solutions were titrated with water used as nonsolvent under stirring. The distilled water was added to the polymeric solution drop by drop until the homogeneous solution became cloudy. Once this turbidity was maintained for at least 30 min during mechanical stirring, the composition was considered a cloud point.

2.3.2 Thickness measurement

The thickness measurement for each sample was performed by using a digital micrometer (Chronos®) with 0.001 mm resolution. In order to be assure the accuracy of the layer thickness, the investigation was carried out at five different points of the prepared MPL. An average thickness value was obtained from the five measured values.

2.3.3 Surface roughness measurement

A surface profilometer equipped with a roughness measuring instrument (MarSurf PS 10, GmbH, Germany) and a 2 µm diamond stylus was employed to measure the surface roughness of MPLs. The probe moves perpendicularly to scan along the sample surface under a constant force. The vertical displacement was then measured as a function of tip position. The roughness measurement was repeated three times to obtain an average surface roughness for each sample.

2.3.4 Contact angle measurement

The contact angle measurement was carried out by sessile-drop method, using an optical tensiometer (Attension Instrument, Biolin, Italy) at 20 °C. First, the samples were placed onto a glass plate with flat surface. A deionized water drop of about 3 µm was deposited on the MPL surface by using a syringe. The angle was then measured by a goniometer. In order to calculate the average contact angle, at least five spots of drops were investigated by the above-mentioned measurement.

2.3.5 Resistance measurements

2.3.5.1 Through-plane resistivity measurement

A two-point resistance measurement device (Keithley 2000 Multimeter) was used to measure the through-plane electrical resistance of the MPL samples. The sample was placed between two cylindrical copper plates (surface area of 0.20 cm^2). Before each measurement, the two copper cylindrical plates were cleaned by metal polish wadding to remove any contaminants on the plate surfaces. A dynamometric screwdriver was employed with a torque moment of 30 cNm to clamp the MPL sample between the two plates. A current was applied through the system and the voltage drop across the MPL sample was then measured. The sample thickness was again checked by using the digital micrometer. Hence, the resistivity can be calculated as the following equation:

$$\sigma = \frac{R.A}{t}$$

Where R is the obtained resistance in Ω, A is the area of the MPL sample in square meter, t is the thickness value of the MPL in meter, as a consequence σ is the resistivity in Ω.m.

2.3.5.2 In-plane resistivity measurement

A four-point probe setup built in-house as illustrated as Figure 8 was used to measure the in-plane resistivity of the MPL samples. A direct current of 1 mA was passed through the two outer probes by using a Keithley 224 programmable current source, Keithley Instruments Inc. A Keithley 2182 Nanovoltmeter was utilized to measure the voltage across the MPL.

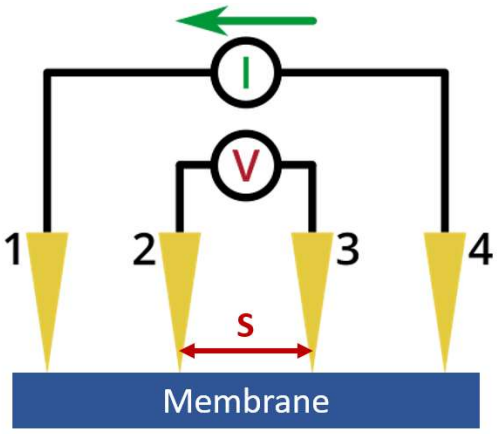

Figure 8: Four-point probe setup for in-plane resistivity measurement

In principle, the sheet resistance of MPL was measured by applying the current through the outer probes and checking the voltage across the inner probes. The resistance was then calculated by the Ohm's Law:

$$R = \frac{V}{I}$$

Where I is the applied current in Ampere and V is the obtained voltage in Volts.

Hence, the resistivity can be computed as an equation below:

$$\sigma = \frac{R.A}{s}$$

Where R is the calculated resistance above in Ω, s is the distance between the two inner probes in meter, A is the area of the MPL sample in square meter which can be determined by the sample thickness multiplied by the distance between the two inner probes, and as a consequence, the unit of the obtained resistivity is in Ω.m.

2.3.6 Through-plane air permeability measurement

Through-plane air permeability was examined by using an in-house built setup which is described in Figure 9.

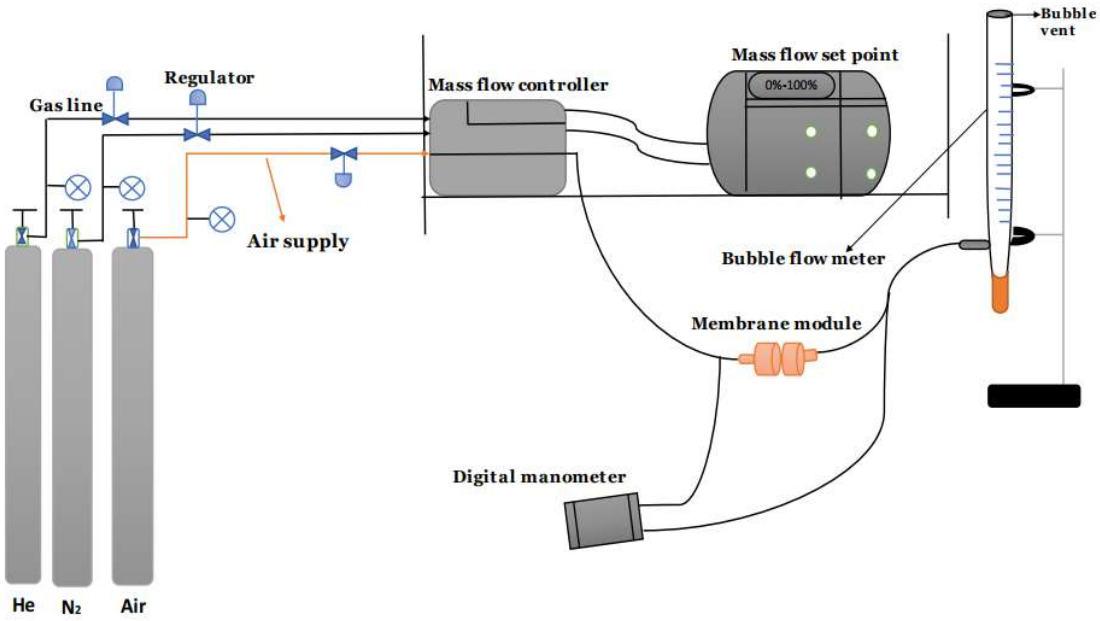

Figure 9: Through-plane gas permeability measurement setup[5]

The air permeance measurement was conducted at room temperature. A certain airflow rate was first preset by using a mass flow controller (Brooks Mass Flow Controllers 5820E Series), a corresponding pressure drop through MPL was then measured by a digital differential pressure transducer (Testo 520). The air flow rate after passing through the MPL was confirmed by using a bubble soap flowmeter. The MPL samples were assembled with the MPL side at the inlet in the sample cell. The active area of MPL samples was 0.80 cm^2.

The air molar permeance (mol m^{-2} s^{-1} Pa^{-1}) was as equation below:

$$Air\ permeance = \frac{J}{\Delta P}$$

Where J is molar flow rate computed by mass transfer to unit sample area and ΔP is the obtained pressure drop.

The MPL air mola permeability (mol m^{-1} s^{-1} Pa^{-1}) was calculated by measuring the sample thickness:

$$Air\ permeability = Air\ permeance * thickness$$

2.3.7 Total porosity

Porosity of the MPL samples is denoted the volume space of the pores in the specimen divided by the total volume of the specimen. The measurement can be conducted by impregnation the MPL specimen into 1-octanol bath[18] as wetting liquid since the MPL is hydrophobic. The weight values of MPL samples before and after immersion were then confirmed. The porosity (%) can be computed as following formula[19]:

$$Porosity\ (\%) = \frac{V_{empty}}{V_{total}} = \frac{W_{wet} - W_{dry}}{V_{dry} \times \rho_{octanol}}$$

Where W_{wet} and W_{dry} denoted as the weights of specimen before and after immersion into 1-octanol bath, V_{dry} = A x l and corresponds to the specimen volume in the dry state with A is the MPL specimen area and l is the specimen thickness, and $\rho_{1\text{-octanol}}$ is the density of 1-octanol (0.824g.cm^{-3}).

2.3.8 Average pore size

In order to evaluate the active pores (pores which actively contribute to the mass transfer of the fluid) in the MPL sample, the liquid-liquid displacement porosimetry was used. An experimental apparatus can be illustrated in Figure 10.

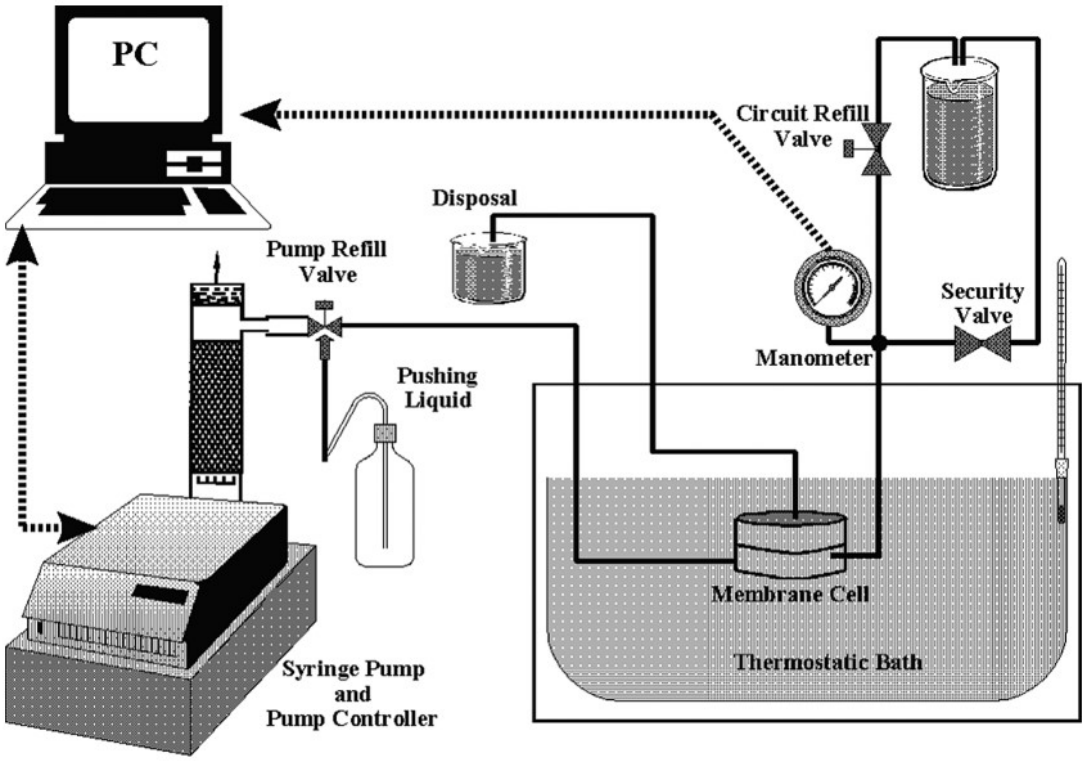

Figure 10: Scheme of apparatus for liquid-liquid displacement porosimetry measurement[20]

A 1:1 w/w mixture of water/1-octanol has been used due to possessing low interfacial tension. In principle, by monitoring the pressure drop corresponding to the flow through the MPL, a pore size distribution can be obtained using Washburn equation:

$$\Delta p = \frac{2\gamma cos\theta}{r_p}$$

Where Δp is the pressure drop, γ is the interfacial tension of the liquid mixture (8.5 $mN.m^{-1}$), θ is the contact angle between the MPL and the liquid-liquid interface (assumed to be zero), and r_p is the equivalent pore radius. Considering cylindrical pores, the Hagen–Poiseuille equation can be used to correlate the volumetric flow, Q, and the number of pores, n, having a given pore radius, r at each flow-pressure couple measured and a pore size distribution can be derived.

2.3.9 Field emission Scanning electron microscopy (FE-SEM)

Field emission scanning electron microscopy (FE-SEM Zeiss SUPRA 40 VP) was utilized to investigate the morphology of the MPL samples. The acceleration voltage was set at 5kV. To study the MPL morphology at the surface, the MPL sample was adhered to a stub and coated with a thin carbon film to eventually improve its electrical conductivity. In order to prepare for cross-sectional investigation, the MPL samples were fractured by freezing in liquid nitrogen for 30 min. The morphology of the MPLs was then observed at both surface and cross-section.

2.3.10 PEM fuel cell test of the MPL samples

A single cell performance of the MPL samples was investigated by using the PEMFC hardware as illustrated in Figure 11.

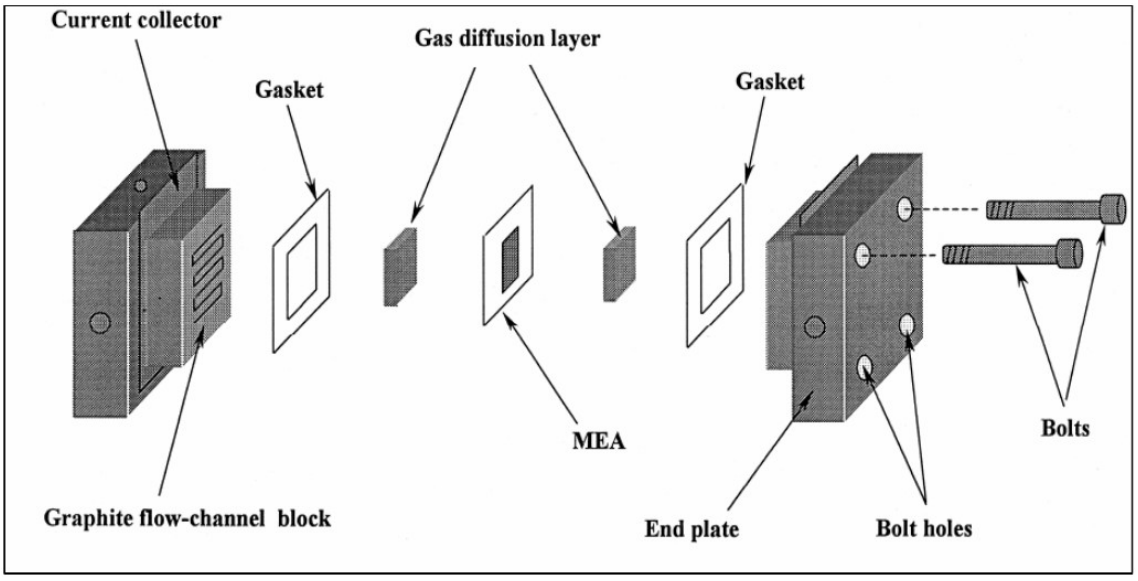

Figure 11: PEMFC component schematic[21]

The design of single PEM fuel cell consists of current collectors, end plates, bolt holes and bolts, graphite plates, gaskets, gas diffusion layers, and a commercial catalyst coated polymer electrolyte membrane. In the above set-up, the catalyst coated membrane was composed of Nafion®212 membrane (Chemours®) with a Pt loading of ~0.5$mg.cm^2$ for both anode and cathode sides. Active area of the single cell was 5 cm^2. The prepared MPL were placed on the anode side while a commercial electrode (ELAT) was at the cathode side. Pure hydrogen and air were fed to the fuel cell. The flow rate of reactant gases was kept at 50 $g.h^{-1}$ for hydrogen and at 15 $g.h^{-1}$ for air. The humidification temperature of air and hydrogen was maintained at 26.2 °C as well as the PEMFC to ensure a 100% relative humidity. . By application of an electric load to the PEMFC the corresponding current and voltage values were measured simultaneously in order to build the polarization curve. .

Chapter 3: Results and discussion

3.1 Cyrene as green solvent

Replacing other toxic solvents by Cyrene referred as a bio-based solvent in order to dissolve PVDF has been faced many challenges. In this work, we have been striving for dissolving PVDF in Cyrene. According to thermodynamic point of view, dissolution of the polymer can be explained by Gibbs free energy which depends on temperature by equation as below:

$$\Delta G_{mix} = \Delta H_{mix} - T\Delta S_{mix}$$

The dissolution of an amorphous polymer into a solvent can be regarded as a process with slightly entropic increase. The higher the temperature heating for the polymer mixture, the lower the value of Gibbs free energy is. It should be noted that polymer dissolution is governed by both thermodynamic and kinetic effects. Herein, increasing the temperature of the mixture facilitates the diffusion of the solvent into the polymer bulk[17], resulting in the complete polymer dissolution.

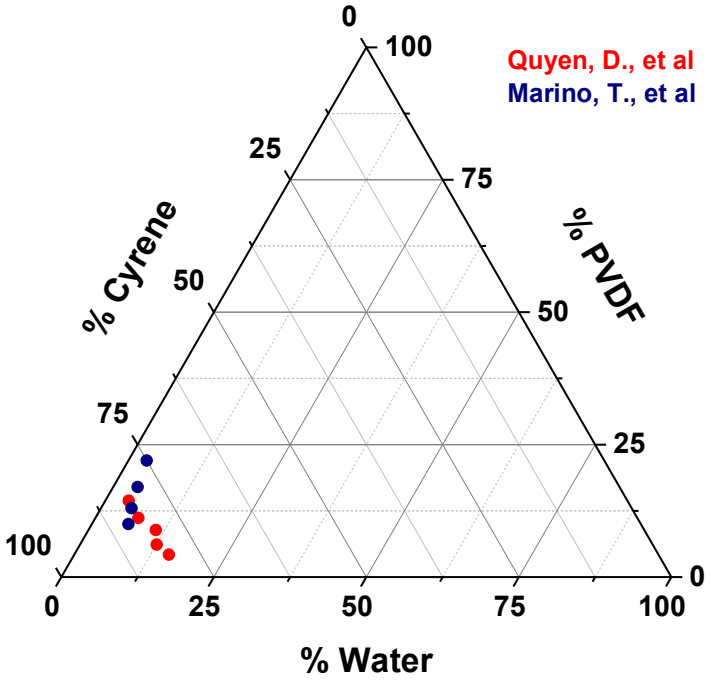

Figure 12: Schematic ternary phase diagram of the PVDF/Cyrene/Water system obtained from this work (Quyen, D., et al.) and the published report (Marino, T., et al.)[16]

In order to estimate the morphology of the MPL, the ternary phase diagram was constructed as a key role. Here, the binodal curve in the diagram was derived from the cloud point measurement, as shown in Figure 12. Combining data obtained from this work and Marino's report, the binodal curve was situated close to the solvent/polymer axis. This verifies less thermodynamic stability of the polymeric solution, as consequence, the demixing process can easily be occurring by adding a small amount of nonsolvent. In the PVDF/Cyrene/Water system, the higher the concentration of PVDF in solution, the smaller the water required for inducing the demixing process.

The morphology of PVDF-based layers without addition of CB on the carbon paper support was investigated by Field emission scanning electron microscopy. FE-SEM images of top surface and cross section of PVDF-based film are shown in Figure 13.

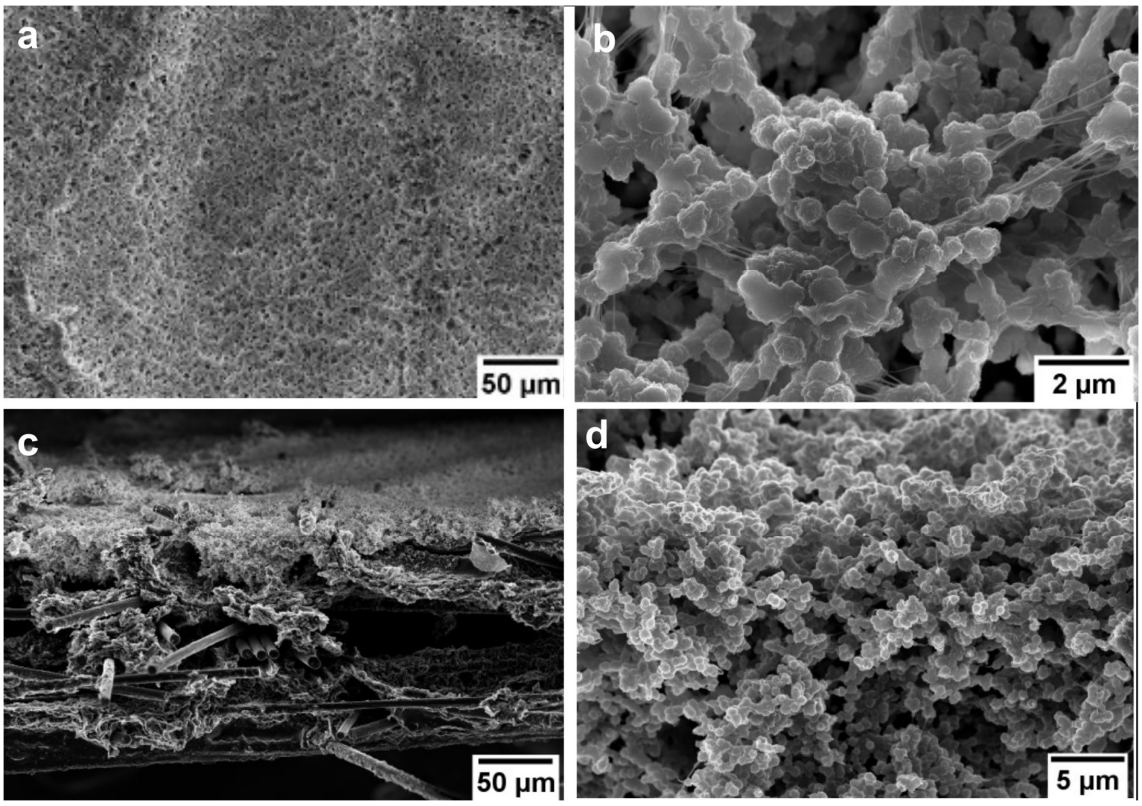

Figure 13: FE-SEM images of a,b surface and c,d cross-sections of PVDF-based porous layer without adding CB as filler.

As illustrated in Figure 13, the morphology of PVDF-based film was obtained with spherulitic microparticles linked through fiber-like connection. This can be attributed to the high temperature used for preparing the polymeric solution. The higher the temperature of the mixing process, the shorter the precipitation time of PVDF is[22]. Based on that, lowering the precipitation time results in the PVDF-based layer easier to be precipitated from the vapor phase. It also needs to be considered that the surface of the spherulites is rough and not smooth which induces increase of the hydrophobicity.

3.2 Effect of CB:PVDF ratios on the MPL properties

The influence of CB content on hydrophobicity of the MPL samples was studied by contact angle and surface roughness measurement which are shown in Figure 14. It should be noted that the hydrophobicity of material itself and roughness of MPL surface influences on the contact angle. PVDF-based porous membranes or layers exhibit high hydrophobicity (contact angle > 90°) due to their fluorinated composition. Fluoropolymers possess the element fluorine which gives strong electronegative characteristics, as a consequence, show low surface energy[23]. Thanks to hydrophobicity of the PVDF-based material itself, the higher the surface roughness, the higher contact angle value is[24]. In Figure 14, all MPL samples were verified with high hydrophobicity via the high water contact angle values (> 135°). In this case, the effect of surface roughness on the contact angle is negligible. Also, the different CB amounts added to the slurry induce no impact on the hydrophobicity of MPL samples.

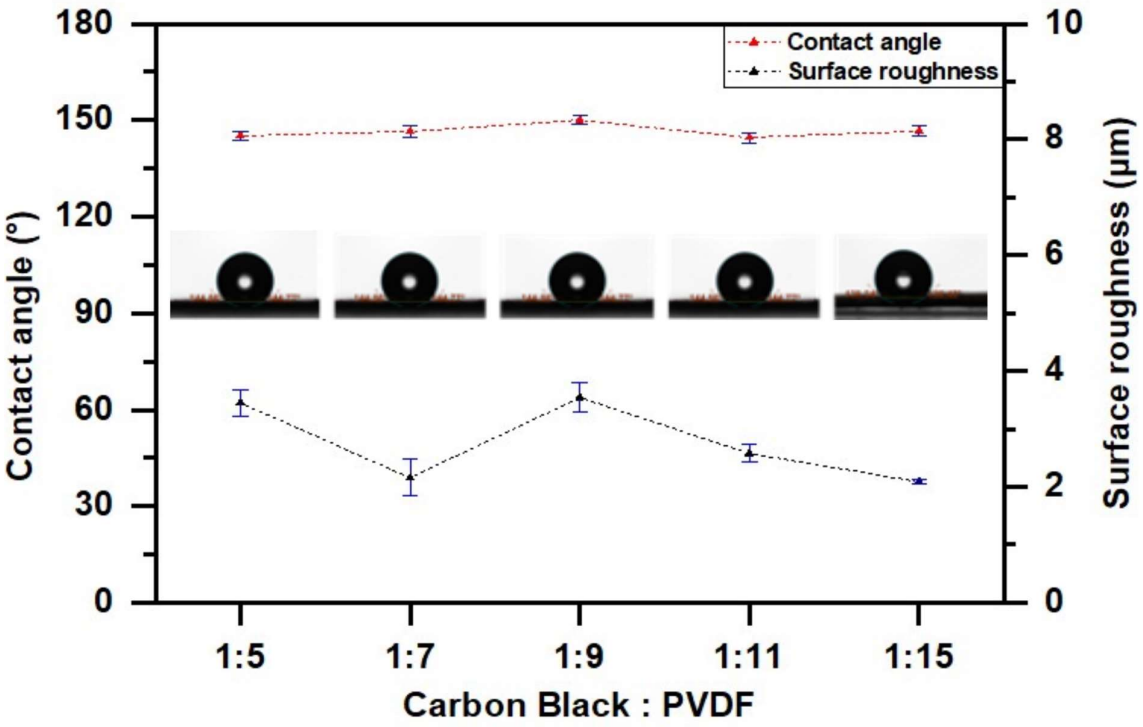

Figure 14: Effect of CB:PVDF ratios on surface roughness and contact angle

In order to achieve a good performance in fuel cells application, the MPL samples are required to possess good electrical conductivity and air permeability. The effect of different CB:PVDF ratios on both the through-plane electrical resistance and air permeability is shown in Figure 15.

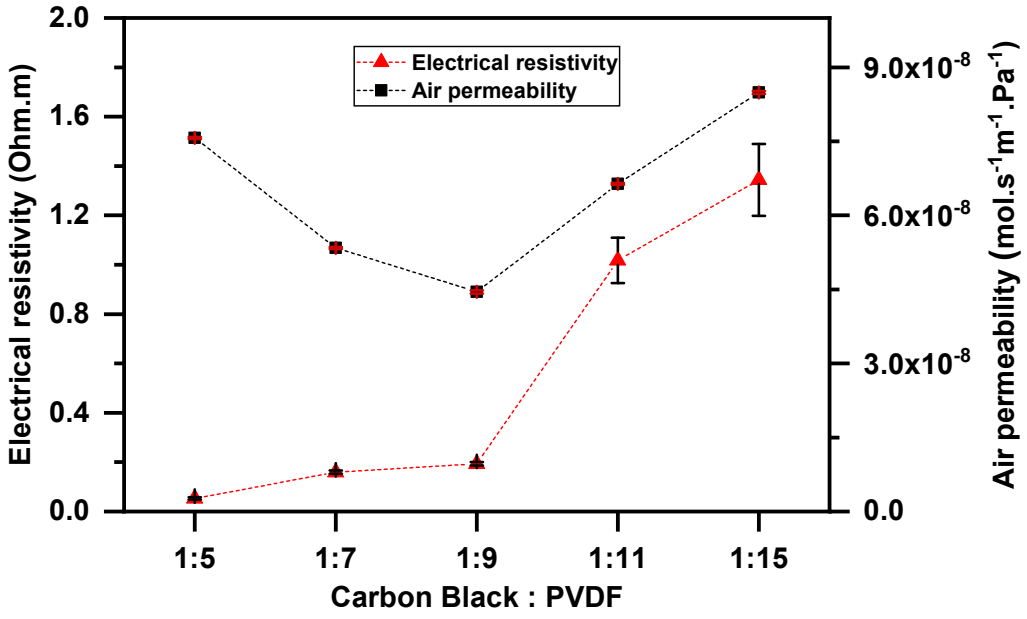

Figure 15: Effect of CB:PVDF ratios on through-plane electrical resistivity and air permeability

As expected, the electrical resistivity increases as the amount of CB decreases. The fluctuation of air permeability can be attributed to the porosity of MPL samples. In this work, both the filler content in slurry and solvent-nonsolvent exchange process are crucial contribution to the pore formation. The situation is more complex when CB is used as filler.

First, the higher the CB amount in slurry, the higher the void content is[25]. This can be demonstrated by the first trend of air permeability which is corresponds to the decrease line from 1:5 to 1:9 of CB:PVDF ratio. However, CB is also well-known as naturally hydrophobic material. Herein, water plays a role as non-solvent in the phase separation process. Presence of CB induces prevention of water flow penetrating into layer structure and exchange with solvent. The lower the solvent-nonsolvent exchange rate, the lower the pore size in the polymeric porous layer is[26]. In Figure 15, the second trend exhibits a good agreement with the above-mentioned point of view. By lowering the CB amount in slurry, the MPL samples show better in the air permeability.

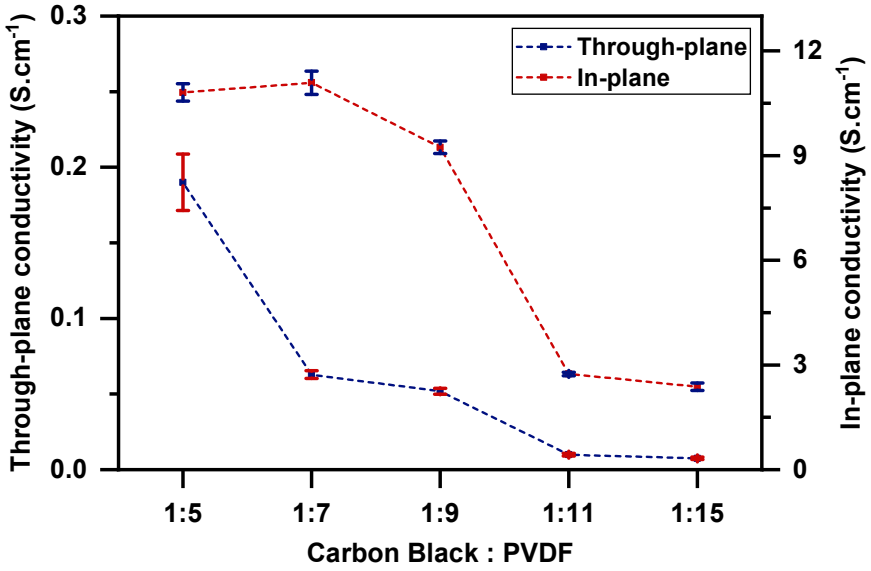

Figure 16: Effect of CB:PVDF ratios on through-plane and in-plane conductivity

In theory, adding CB in the slurry could help to increase the electrical conductivity of MPL samples. The influence of CB:PVDF ratios on through-plane and in-plane conductivity of the samples is illustrated in Figure 16. Here, the lower the CB amount, the lower the electrical conductivity is. As shown in Figure 16, the conductivity values in through-plane measurement are generally two orders of magnitude lower than that of in-plane case. This can be explained due to anisotropy of the Carbon fiber support which possesses a different degree of the Carbon fiber connection[27, 28].

The top surficial and cross-sectional SEM images were collected for the MPL samples with the CB:PVDF ratios as 1:5 and 1:15 which is shown in Figure 17. The MPL film with the CB:PVDF ratio of 1:15 was obtained with larger pore size compared to the sample with that of 1:5. This observation is in a good agreement with the values obtained from the air permeability measurement.

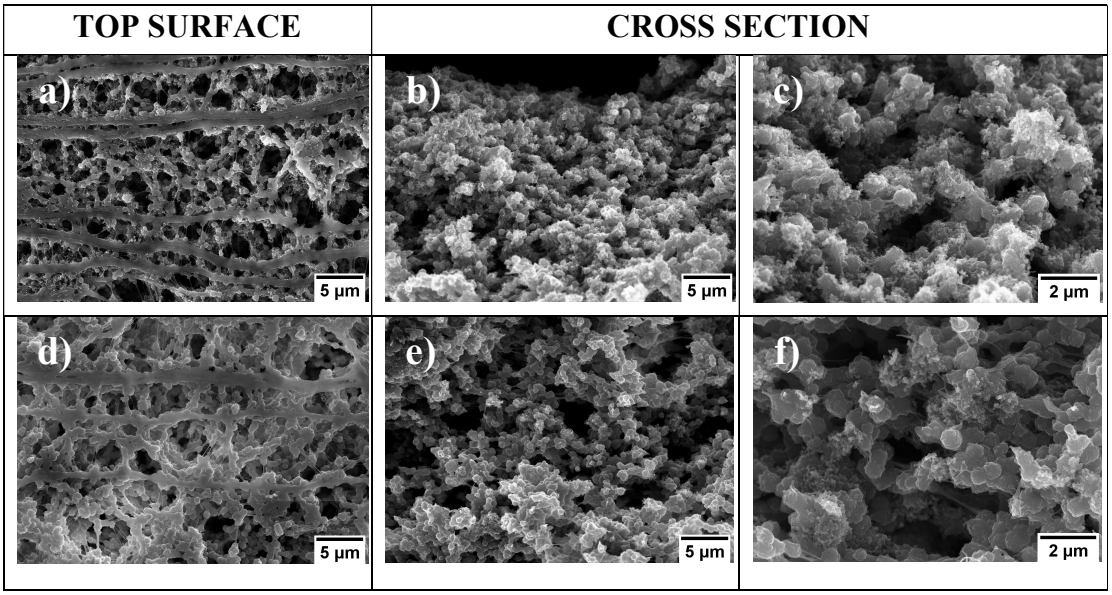

Figure 17: SEM images a,b,c sample with ratio 1:5 of CB:PVDF; d,e,f sample with ratio 1:15 of CB:PVDF

Hence, considering the combination of the above-obtained results and the necessary requirements for fuel cell application, the MPL with the CB:PVDF ratio of 1:5 is potential and outstanding among the five different MPL samples. This sample was then analyzed by the liquid-liquid displacement porosimetry measurement in order to evaluate the active pores in the MPL.

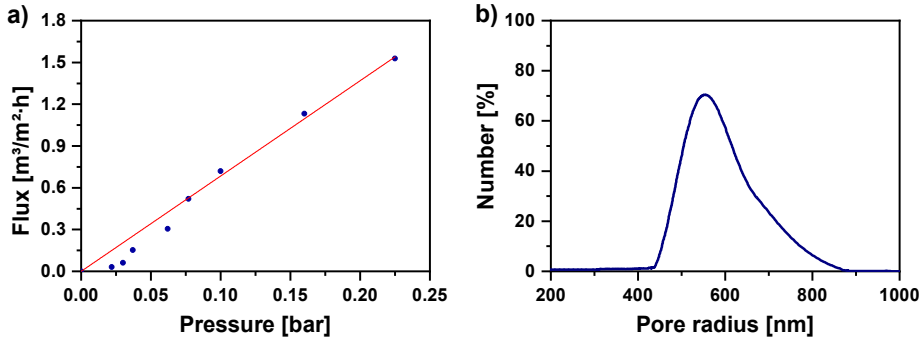

Figure 18: Typical porosimetric run (a) and pore-size distribution (b) of the MPL film with the CB:PVDF ratio of 1:5

The results obtained from the porosimetric run and computed by the Washburn equation are shown in Figure 18. The given MPL was demonstrated as containing mostly pores with a pore radius of 0.54 µm.

3.3 Effect of coagulation bath conditions on the MPL properties

In the non-solvent induced-phase inversion method, the coagulation bath plays as an important role to the solvent-nonsolvent exchange process. There are two main factors affecting to the structure and pore size of the MPL which include the nonsolvent choice and the temperature of the coagulation bath. In this work, five different conditions of the coagulation bath were used to investigate characteristics of the resulting MPL layers.

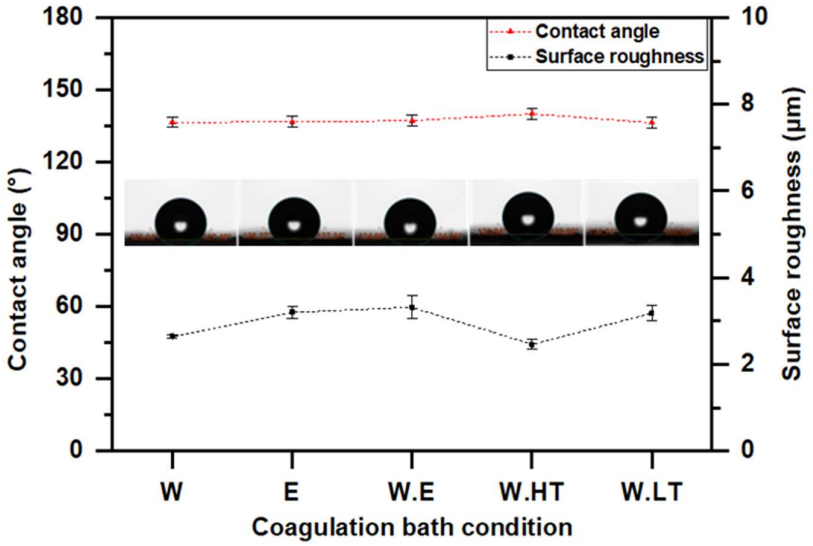

Figure 19: Effect of coagulation bath conditions on the contact angle

First, the MPL samples obtained after immersing into the different coagulation bath were investigated their hydrophobicity by the contact angle and surface roughness measurement. The results were shown in Figure 19.

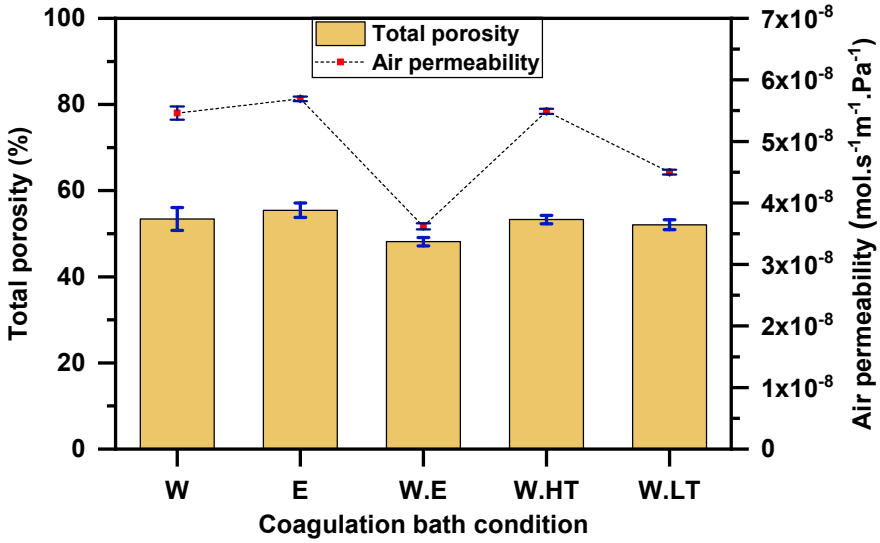

Figure 20: Effect of coagulation bath conditions on porosity and air permeability

The appropriateness of solvent and nonsolvent is crucial for the demixing process. During the exchange process, the nonsolvent (water or ethanol) penetrates into the polymeric solution and the solvent (Cyrene) moves forward the nonsolvent. Based on the types of nonsolvent, the hydrophobicity can differently be obtained. For instance looking at the literature about porous membranes, symmetric membranes (ethanol used as nonsolvent) exhibit higher hydrophobicity compared to that of asymmetric membranes (water used as nonsolvent)[29]. Also, the bath temperature is considered as the higher the bath temperature, the higher the MPL pore size is[30]. In Figure 19, all five MPL samples were observed with high hydrophobicity corresponding to the contact angle of higher than 130°. There is no significant difference among the MPL films which can be attributed to the high hydrophobicity of the original PVDF-based membranes.

A study by Tomaszewska et al indicated that the membrane with porous structure can be formed by slow coagulation[31]. The different coagulants possess their own coagulation ability which can be shown via the difference in the solubility parameters between the coagulant and polymer ($\Delta\delta_{c\text{-}p}$)[32]:

$$\Delta\delta_{c-p} = \sqrt{\left(\delta_{d,c} - \delta_{d,p}\right)^2 + \left(\delta_{p,c} - \delta_{p,p}\right)^2 + \left(\delta_{h,c} - \delta_{h,p}\right)^2}$$

Where $\delta_{i,c}$ (i=d,p,h) are the Hansen solubility parameters of the coagulant ($MPa^{1/2}$) and δi,p (i=d,p,h) are the Hansen solubility parameters of the polymer ($MPa^{1/2}$).

The weaker the coagulation ability, the slower the precipitation rate is. The influence of coagulation bath conditions on the porosity of MPL membranes was also investigated, as shown in Figure 20. In the case of PVDF solution, water ($\Delta\delta_{c\text{-}p}$ = 33.43 $MPa^{1/2}$) exhibits stronger coagulation ability than that of ethanol ($\Delta\delta_{c\text{-}p}$ = 10.94 $MPa^{1/2}$)[33]. Nevertheless, there is no significant change in both air permeability and total porosity obtained from the five different MPL samples. In conclusion, the porosity of prepared MPL films does not strongly depend on the coagulation bath conditions.

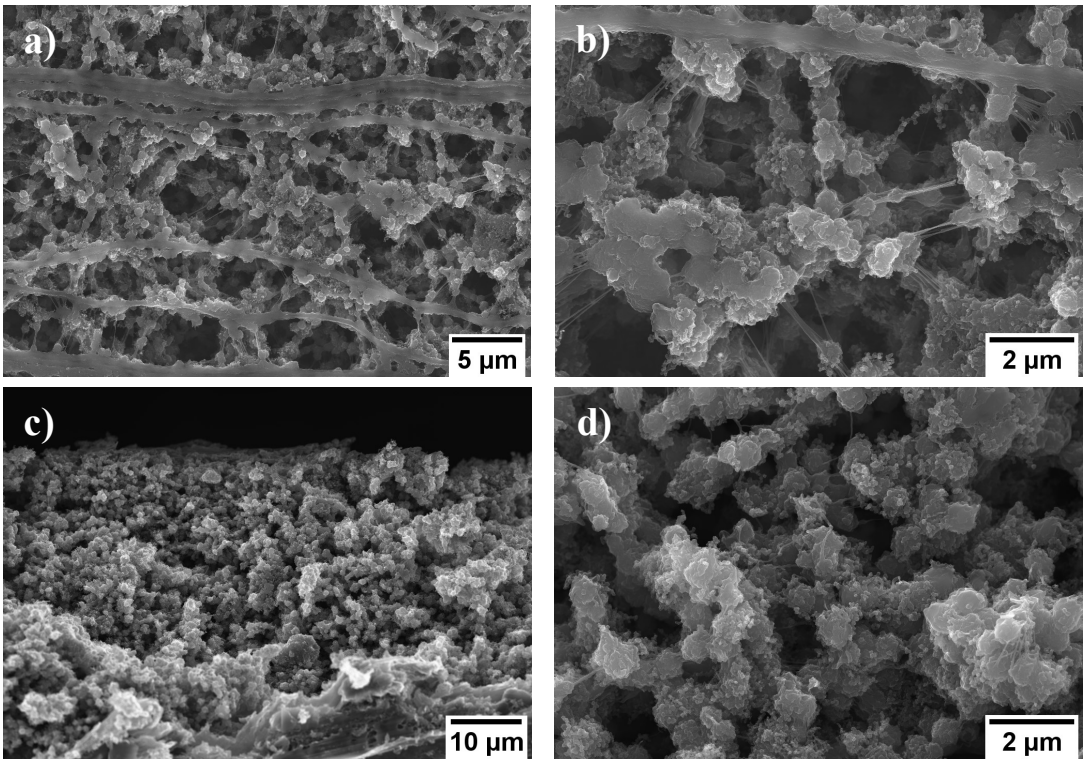

Figure 21: SEM images of a,b surface and c,d cross-sections of sample labeled W

Aiming to develop of environmentally friendly approach, the coagulation bath containing water as nonsolvent at room temperature was considered as the best choice. The morphology of resulting membrane labeled W was then investigated by SEM images which are shown in Figure 21. The MPL film exhibits a good porous structure thanks to the original PVDF-based membrane.

3.4 PEM fuel cell test of the MPL samples

The PEMFC performance of the studied MPL samples was investigated and all obtained results were summarized in the polarization and power density curves reported in Figure 22. As expected, the performance of the studied fuel cells depends proportionally on the amount of carbon black. The higher the carbon black content, the better the PEMFC performance was achieved.

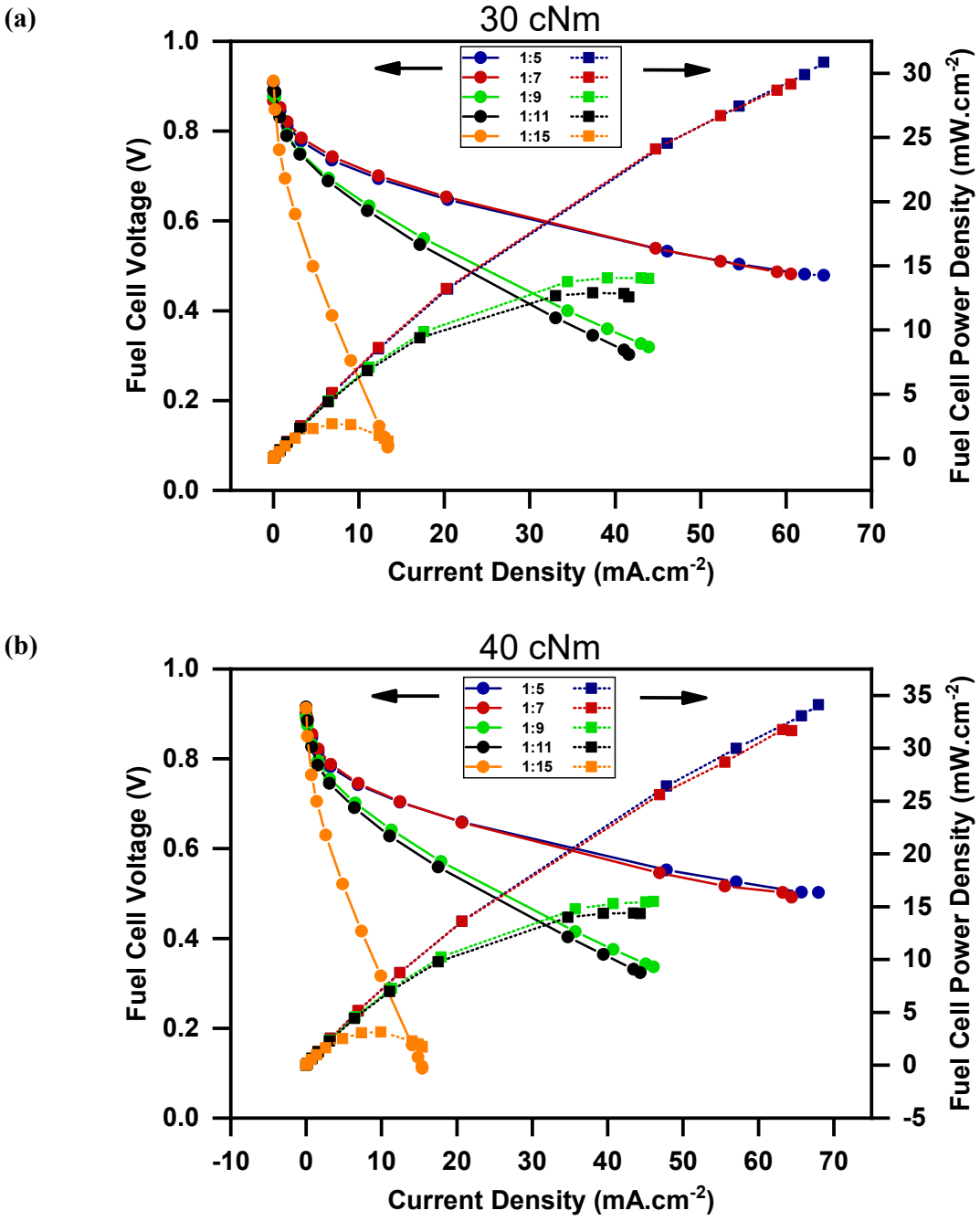

Figure 22: Effect of mechanical compression on the PEMFC performance of the studied MPL samples with different CB:PVDF ratios: a) 30 cNm and b) 40 cNm

The MPL with the lowest CB content (1:15) shows a rapid decrease of the voltage with the increasing current density and a lower power density maximum at relatively low current density indicating that the MPL is clearly affected by a strong ohmic resistance which can be attributed to the very low electrical conductivity. The MPLs with ratio of CB 1:5 and 1:7 showed the the best performance which was comparable. These two MPLs satisfy both the low resistance and good gas permeability. Applying an optimal compression force could assist the PEM fuel cell to achieve the best performance. Low the compression forces makes the PEMFC may suffer from increased ohmic loss, while the PEMFC with high compression forces can suffer from pressure or concentration losses. In this study, the

performance of fuel cells was better after being compressed with 40 cNm. It can clearly be observed by higher values of power density in the case of being compressed with torque value of 40 cNm compare to those of 30 cNm.

Conclusion and perspective

In this project, Cyrene as a bio-based solvent was successfully used to dissolve the PVDF. Herein, the microporous layer (MPL) was prepared via the nonsolvent-induced phase separation (NIPS) technique for proton exchange membrane fuel cell (PEMFC) application. The experimental data were discussed with respect to the ternary phase diagram, contact angle, roughness, membrane morphology, air permeance, porosity, and pore size distribution. Influence of polymer/filler ratio and coagulation bath conditions on characteristics of the MPL was thoroughly analyzed.

In the PVDF/Cyrene/Water system, the higher the concentration of PVDF in solution, the smaller the water required for inducing the demixing process. The morphology of PVDF-based films was obtained with spherulitic microparticles linked through fiber-like connection. This can be attributed to the high temperature was used for preparing the polymeric solution. All MPL samples were verified with high hydrophobicity via the high water contact angle values (> 135°). As expected, adding CB in the slurry could help to increase the electrical conductivity of MPL samples. The MPL membrane with the CB:PVDF ratio of 1:5 was demonstrated as containing mostly small pores with a pore radius of 0.54 μm. The porosity of prepared MPL films does not strongly depend on the coagulation bath conditions. The PEMFC performance of the studied MPL samples depends proportionally on the amount of carbon black. The higher the carbon black content, the better the PEMFC performance was achieved. Also, applying an optimal compression force could assist the PEM fuel cell to achieve the best performance since it probably improves the contact without to be very detrimental for the gas permeability.

Bibliography

1. Niya, S. M. R.; Hoorfar, M., Study of proton exchange membrane fuel cells using electrochemical impedance spectroscopy technique–A review. *Journal of Power Sources* **2013,** *240*, 281-293.
2. Ong, A. L.; Bottino, A.; Capannelli, G.; Comite, A., Effect of preparative parameters on the characteristic of poly (vinylidene fluoride)-based microporous layer for proton exchange membrane fuel cells. *Journal of Power Sources* **2008,** *183* (1), 62-68.
3. Cindrella, L.; Kannan, A. M.; Lin, J.; Saminathan, K.; Ho, Y.; Lin, C.; Wertz, J., Gas diffusion layer for proton exchange membrane fuel cells—A review. *Journal of Power Sources* **2009,** *194* (1), 146-160.
4. Kraytsberg, A.; Ein-Eli, Y., Review of advanced materials for proton exchange membrane fuel cells. *Energy & Fuels* **2014,** *28* (12), 7303-7330.
5. Mideksa, E. A. Development of nanocomposite hydrophobic polymer-based porous structures for Polymer electrolyte membrane fuel cells. University of Genoa, 2021.
6. Badea, N. I., Hydrogen as Energy Sources—Basic Concepts. *Energies* **2021,** *14* (18), 5783.
7. Mauritz, K. A.; Moore, R. B., State of understanding of Nafion. *Chemical reviews* **2004,** *104* (10), 4535-4586.
8. Islam, M. N.; Shrivastava, U.; Atwa, M.; Li, X.; Birss, V.; Karan, K., Highly ordered nanoporous carbon scaffold with controllable wettability as the microporous layer for fuel cells. *ACS applied materials & interfaces* **2020,** *12* (35), 39215-39226.
9. Borup, R. L.; Vanderborgh, N. E., Design and testing criteria for bipolar plate materials for PEM fuel cell applications. *MRS Online Proceedings Library (OPL)* **1995,** *393*.
10. Nagai, Y.; Eller, J.; Hatanaka, T.; Yamaguchi, S.; Kato, S.; Kato, A.; Marone, F.; Xu, H.; Büchi, F. N., Improving water management in fuel cells through microporous layer modifications: Fast operando tomographic imaging of liquid water. *Journal of Power Sources* **2019,** *435*, 226809.
11. Manzi-Orezzoli, V.; Siegwart, M.; Scheuble, D.; Chen, Y.-C.; Schmidt, T. J.; Boillat, P., Impact of the microporous layer on gas diffusion layers with patterned wettability I: material design and characterization. *Journal of The Electrochemical Society* **2020,** *167* (6), 064516.
12. Critchlow, G. W.; Litchfield, R. E.; Sutherland, I.; Grandy, D. B.; Wilson, S., A review and comparative study of release coatings for optimised abhesion in resin transfer moulding applications. *International journal of adhesion and adhesives* **2006,** *26* (8), 577-599.
13. Dong, X.; Lu, D.; Harris, T. A.; Escobar, I. C., Polymers and solvents used in membrane fabrication: a review focusing on sustainable membrane development. *Membranes* **2021,** *11* (5), 309.
14. Guillen, G. R.; Pan, Y.; Li, M.; Hoek, E. M., Preparation and characterization of membranes formed by nonsolvent induced phase separation: a review. *Industrial & Engineering Chemistry Research* **2011,** *50* (7), 3798-3817.
15. Sherwood, J.; Constantinou, A.; Moity, L.; McElroy, C. R.; Farmer, T. J.; Duncan, T.; Raverty, W.; Hunt, A. J.; Clark, J. H., Dihydrolevoglucosenone (Cyrene) as a bio-based alternative for dipolar aprotic solvents. *Chemical Communications* **2014,** *50* (68), 9650-9652.
16. Marino, T.; Galiano, F.; Molino, A.; Figoli, A., New frontiers in sustainable membrane preparation: Cyrene™ as green bioderived solvent. *Journal of Membrane Science* **2019,** *580*, 224-234.
17. Marshall, J. E.; Zhenova, A.; Roberts, S.; Petchey, T.; Zhu, P.; Dancer, C. E.; McElroy, C. R.; Kendrick, E.; Goodship, V., On the solubility and stability of polyvinylidene fluoride. *Polymers* **2021,** *13* (9), 1354.
18. Pagliero, M.; Bottino, A.; Comite, A.; Costa, C., Novel hydrophobic PVDF membranes prepared by nonsolvent induced phase separation for membrane distillation. *Journal of Membrane Science* **2020,** *596*, 117575.

19. Guo, Z.; Xiu, R.; Lu, S.; Xu, X.; Yang, S.; Xiang, Y., Submicro-pore containing poly (ether sulfones)/polyvinylpyrrolidone membranes for high-temperature fuel cell applications. *Journal of Materials Chemistry A* **2015,** *3* (16), 8847-8854.
20. Sanz, J. M.; Jardines, D.; Bottino, A.; Capannelli, G.; Hernández, A.; Calvo, J. I., Liquid–liquid porometry for an accurate membrane characterization. *Desalination* **2006,** *200* (1-3), 195-197.
21. Wang, Y. Conductive thermoplastic composite blends for flow field plates for use in polymer electrolyte membrane fuel cells (PEMFC). University of Waterloo, 2006.
22. Strathmann, H.; Kock, K., The formation mechanism of phase inversion membranes. *Desalination* **1977,** *21* (3), 241-255.
23. Moradi, R.; Karimi-Sabet, J.; Shariaty-Niassar, M.; Koochaki, M. A., Preparation and characterization of polyvinylidene fluoride/graphene superhydrophobic fibrous films. *Polymers* **2015,** *7* (8), 1444-1463.
24. Li, C.; Zhang, J.; Han, J.; Yao, B., A numerical solution to the effects of surface roughness on water–coal contact angle. *Scientific Reports* **2021,** *11* (1), 1-12.
25. Beard, K. W.; Edwards, A. M., Filled porous membrane. Google Patents: 2016.
26. Tasselli, F., Non-solvent induced phase separation process (NIPS) for membrane preparation. *Encycl Membr* **2014**, 1-3.
27. Ahadi, M.; Tam, M.; Stumper, J.; Bahrami, M., Electronic conductivity of catalyst layers of polymer electrolyte membrane fuel cells: Through-plane vs. in-plane. *international journal of hydrogen energy* **2019,** *44* (7), 3603-3614.
28. Nascimento, J. F.; Ezquerra, T.; Baltà-Calleja, F.; Seferis, J., Anisotropy of electrical conductivity and structure in polymer-carbon fiber composite materials. *Polymer composites* **1995,** *16* (2), 109-113.
29. Thürmer, M. B.; Poletto, P.; Marcolin, M.; Duarte, J.; Zeni, M., Effect of non-solvents used in the coagulation bath on morphology of PVDF membranes. *Materials Research* **2012,** *15* (6), 884-890.
30. Zare, S.; Kargari, A., Membrane properties in membrane distillation. In *Emerging Technologies for Sustainable Desalination Handbook*, Elsevier: 2018; pp 107-156.
31. Tomaszewska, M., Preparation and properties of flat-sheet membranes from poly (vinylidene fluoride) for membrane distillation. *Desalination* **1996,** *104* (1-2), 1-11.
32. Seferis, J.; Brandrup, J.; Immergut, E., Polymer handbook. *Wiley, New York, ed* **1989,** *3*, 45.
33. Li, Q.; Xu, Z. L.; Liu, M., Preparation and characterization of PVDF microporous membrane with highly hydrophobic surface. *Polymers for Advanced Technologies* **2011,** *22* (5), 520-531.